Picosecond Dynamics of the Prototropic Reactions of 7-Hydroxyflavylium Photoacids Anchored at an Anionic Micellar Surface

ARTICLE *in* THE JOURNAL OF PHYSICAL CHEMISTRY A · MARCH 2010

Impact Factor: 2.69 · DOI: 10.1021/jp100281u · Source: PubMed

4 AUTHORS, INCLUDING:

Frank Quina
University of São Paulo
164 PUBLICATIONS **4,387** CITATIONS
SEE PROFILE

Ana C Fernandes
Technical University of Lisbon
60 PUBLICATIONS **1,221** CITATIONS
SEE PROFILE

Antonio Macanita
Technical University of Lisbon
126 PUBLICATIONS **2,424** CITATIONS
SEE PROFILE

Picosecond Dynamics of the Prototropic Reactions of 7-Hydroxyflavylium Photoacids Anchored at an Anionic Micellar Surface

Adilson A. Freitas,[†] Frank H. Quina,[‡] Ana C. Fernandes,[†] and António A. L. Maçanita*,[†]

Departamento Engenharia Química, Centro de Química Estrutural, IST/UTL, Lisbon 1049-001, Portugal, Instituto de Química, Universidade de São Paulo, CP 26077, São Paulo 05513-970, Brazil

Received: January 11, 2010; Revised Manuscript Received: February 12, 2010

Three water-insoluble, micelle-anchored flavylium salts, 7-hydroxy-3-octyl-flavylium chloride, 4′-hexyl-7-hydroxyflavylium chloride, and 6-hexyl-7-hydroxy-4-methyl-flavylium chloride, have been employed to probe excited-state prototropic reactions in micellar sodium dodecyl sulfate (SDS). In SDS micelles, the fluorescence decays of these three flavylium salts are tetraexponential functions in the pH range from 1.0 to 4.6 at temperatures from 293 to 318 K. The four components of the decays are assigned to four kinetically coupled excited species in the micelle: specifically, promptly deprotonable (AH^{+}*) and nonpromptly deprotonable (AH_h^{+}*) orientations of the acid in the micelle, the base-proton geminate pair (A*···H^+), and the free conjugate base (A*). The initial prompt deprotonation to form the geminate pair occurs at essentially the same rate ($k_d \sim 6-7 \times 10^{10}$ s^{-1}) for all three photoacids. Recombination of the geminate pair is ~3-fold faster than the rate of proton escape from the pair ($k_{rec} \sim 3 \times 10^{10}$ s^{-1} and $k_{diss} \sim 1 \times 10^{10}$ s^{-1}), corresponding to an intrinsic recombination efficiency of the pair of ~75%. Finally, the reprotonation of the short-lived free A* (200−350 ps, depending on the photoacid) has two components, only one of which depends on the proton concentration in the intermicellar aqueous phase. Ultrafast transfer of the proton to water and substantial compartmentalization of the photogenerated proton at the micelle surface on the picosecond time scale strongly suggest preferential transfer of the proton to preformed hydrogen-bonded water bridges between the photoacid and the anionic headgroups. This localizes the proton in the vicinity of the excited base much more efficiently than in bulk water, resulting in the predominance of geminate reprotonation at the micelle surface.

Introduction

Phenolic photoacids, whose acidity often increases by 5−6 orders of magnitude upon photoexcitation, have played an important role in advancing our understanding of the details of proton transfer in aqueous solution.[1−5] Studies of photoinduced proton transfer on the picosecond and femtosecond time scale have resulted in rather detailed models for the initial events involved in proton transfer from photoacids to water.[2,5−7] These include subpicosecond electronic redistribution; proton transfer to water on a picosecond time scale, accompanied by solvation of both the proton and the excited base; and, finally, diffusional separation or reencounter of proton and base on a much longer time scale. As for the precise proton transfer mechanism, the simplest model is that in which the initial proton transfer to an adjacent water molecule produces a geminate proton−base pair, which can then either recombine back to the acid or dissociate into a free proton and base, as indicated in Scheme 1.

This model, which contains three kinetic species, has been used by many groups[3,4,8−11] to analyze fast proton transfer kinetics.[12] A slightly more refined kinetic model, proposed by Huppert and collaborators,[3,4] further factors the geminate excited base−proton pair, (A*···H^+), into contact and solvent-separated pairs, (A*··H^+) and (A*−H^+), respectively.

Clearly, on an ultrafast time scale, the kinetics of the proton transfer process will depend on the local water structure around the photoacid at the moment of excitation and the interplay between proton solvation and proton transport within the hydrogen-bonded water network coupled to the geminate base-proton pair.[2,13−15] In this context, molecular dynamics simulations have provided increasingly detailed pictures of proton transport processes in hydrogen-bonded water networks.[16−18] Particularly interesting are recent simulations of the behavior of protons at water−hydrophobic interfaces[19] and simulations[15] and experimental[14] studies of the influence of added anions on water structure and on fast excited state proton transfer reactions.

SCHEME 1

$$AH^{+*} \underset{k_{rec}}{\overset{k_d}{\rightleftharpoons}} (A^*\ldots H^+) \underset{k_p[H^+]}{\overset{k_{diss}}{\rightleftharpoons}} A^* + H^+$$

Since water is known to be more structured at the ionic micelle−water interface,[20] where there is also water−hydrophobic core contact, we have employed in the present work three water-insoluble flavylium salts (Chart 1); namely, 7-hydroxy-3-octyl-flavylium chloride (3-OHF), 4′-hexyl-7-hydroxyflavylium chloride (4′-HHF), and 6-hexyl-7-hydroxy-4-methyl-flavylium chloride (6-HHMF), functionalized with alkyl chains that anchor them at the micellar surface, to examine in detail their excited-state prototropic reactions at the surface of anionic sodium dodecyl sulfate (SDS) micelles. The results are discussed in terms of the relationship between the local water structure and proton transport on the picosecond time scale at the micelle surface.

Experimental Section

Materials and Sample Preparation. The syntheses of 3-OHF, 4′-HHF, and 6-hexyl-7-hydroxy-4-methyl-flavylium chloride have been previously reported.[21] Sodium dodecyl

* Corresponding author. E-mail: macanita@ist.utl.pt.
[†] IST/UTL.
[‡] Universidade de São Paulo.

10.1021/jp100281u
Published on Web 03/03/2010

CHART 1

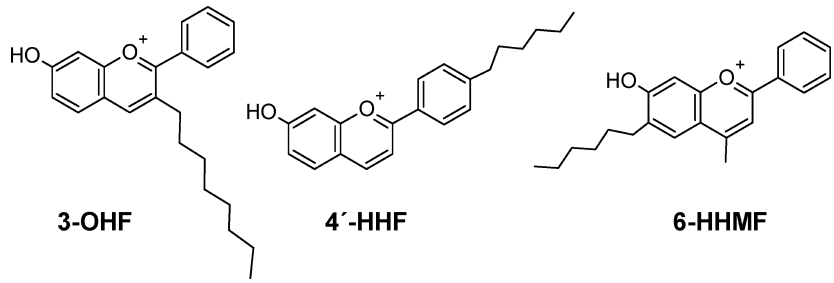

sulfate, minimum 99% (Sigma), and methanol for chromatography (Lab-Scan) were used as received. The water utilized for the preparation of all solutions was deionized by an Elgastat UHQPS system (Elga). For all solutions with pH > 1.0, the ionic strength was maintained constant at 0.10 by appropriate addition of $NaClO_4$. The pH adjustments were made by dilutions of $HClO_4$ and NaOH solutions. The sample concentrations were in the $1-2 \times 10^{-5}$ M range to keep the maximum absorbance of the longest-wavelength absorption band below 0.2.

Measurements. The pH of the solutions was measured at 20 °C using a Crison BasiC 20 pH meter combined with a Mettler Toledo InLab 423 Ag/AgCl microelectrode. UV−vis absorption spectra were collected on a Beckman DU-70 spectrophotometer. Spectra of nonequilibrated solutions of the compounds were measured ~5 s after preparation by adding 2.0 mL of the buffered SDS solution to a dried film of the compound (from a methanol stock solution) in the cuvette. The pH of the solution was verified after running the spectrum. Fluorescence spectra were measured on a SPEX F212l Fluorolog. The spectra were corrected for the wavelength response of optics and photomultiplier.

The fluorescence decays were measured at the magic angle by the time-correlated single photon counting technique, utilizing a Millennia Xs/Tsunami pumping system, from Spectra Physics, as described elsewhere,[22] except for the electronic detection system (SPC-630 board module, from Becker & Hickl GmbH). The board replaces the constant fraction discriminators (CFDs), the time-to-amplitude converter (TAC), the analog-to-digital converter (ADC), and the multichannel analyzer (MCA). The resulting lower electronic time jitter has reduced the pulse fwhm from ~38 to 19 ps (measured at 814 fs/channel).[23] The laser excitation pulse and sample fluorescence emissions were collected using automatic alternate measurement of pulse and sample (2×10^3 counts in the peak channel per cycle) until a total of 10^4 counts had been collected at the maximum. Individual and global analyses of the fluorescence decays, as well as deconvolutions, were carried out with G. Striker's Sand program.[24]

Results

Absorption and Fluorescence Spectra. In aqueous solution, hydroxyflavylium salts, like their naturally occurring analogs the anthocyanins, generally undergo a series of pH-dependent ground state reactions.[25,26] At pH < 2−4 and room temperature, only the cationic form AH^+ is present, whereas at higher pH values, the quinonoidal base A and the hemiketal B are formed. The acid−base equilibrium between AH^+ and A occurs in the microsecond−nanosecond time range,[27,28] while hydration of AH^+ to give B is considerably slower (seconds to minutes).[27] The hemiketal-chalcone tautomerization from B to the (*Z*)-chalcone, C_Z, occurs in the minutes-to-hours time range, and the isomerization of C_Z to the corresponding *E* isomer can take hours or days.[27] In anionic SDS micelles, the foregoing equilibria are substantially modified due to the decrease in the deprotonation[28,29] and hydration rate constants (reflecting selective stabilization of AH^+ at the negatively charged micelle surface) and the increase in the apparent protonation and dehydration rate constants (higher effective local concentration of H^+ at the SDS micellar surface).[28,29] The net result is an increase in the

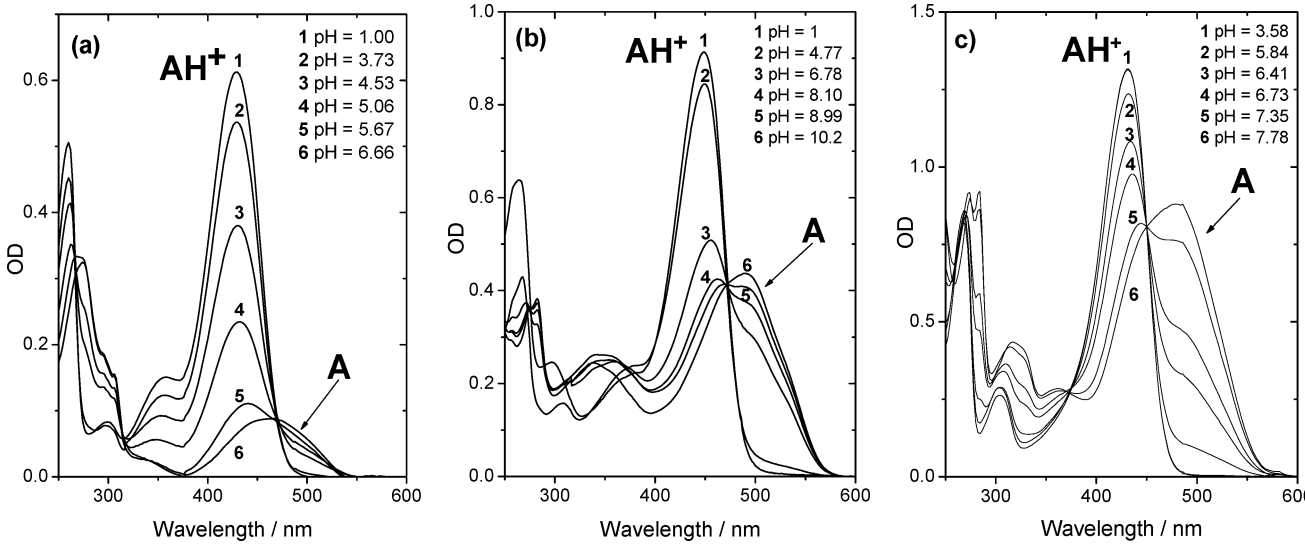

Figure 1. Absorption spectra, taken 5 s after preparation of the solutions, of (a) 3-OHF, (b) 4′-HHF, and (c) 6-HHMF[14] ions in 0.10 M SDS at 20 °C.

TABLE 1: Wavelengths of Maximum Absorption and Fluorescence of the Acid (AH^+) and Base (A) Forms of 3-OHF), 4′-HHF, and 6-HHMF Salts in 0.10 M SDS and Values of the Micelle-Modified pK_a and p$K_{1/2}$

	λmax abs, nm		λmax em, nm			
	AH^+	A	AH^+	A	pK_a	p$K_{1/2}$
3-OHF	428	488	505	615	4.7	4.5
4′-HHF	449	497	504	622	6.0	4.4
6-HHMF	431	480	490	620	6.8[a]	5.1[b]

[a] See ref 30. [b] See ref 21.

apparent acidity (p$K_{1/2}$) and hydration (pK_h) constants upon going from water to SDS micelles.

The functionalized flavylium salts 3-OHF, 4′-HHF, and 6-HHMF are insoluble in water but readily solubilized in micellar SDS solutions.[21] Figure 1 shows absorption spectra of these salts taken 5 s after the preparation of the solutions in 0.10 M SDS at several pH values. At this short delay time, only the flavylium cation AH^+ and the quinonoidal base A are detectable.

Table 1 summarizes the absorption data as well as the micelle-modified pK_a at 20 °C of the three compounds determined from these spectra. The most interesting result is the relatively large difference in the micelle-modified ground state pK_a values of these compounds (ranging from 4.7 to 6.8), which contrasts with the relative insensitivity of the pK_a and p$K_{1/2}$ values of natural and synthetic flavylium salts that do not bear long-chain alkyl substituents attached to the flavylium chromophore (typically ∼4 in water[27,28] and ∼6 in 0.10 M micellar SDS solution[29]).

After attaining thermodynamic equilibrium (∼1 week), the absorption spectra of the same solutions exhibit a decrease in the absorption of the acid and base forms with concomitant formation of the other species (essentially the *trans*-chalcone, C_E, and hemiketal, B, forms) above pH 4. The pH at which half of the acid is converted into products in the equilibrated solutions, referred to as p$K_{1/2}$ and given by the relationship p$K_{1/2}$ = $-\log(K_a + K_h + K_hK_t + K_hK_tK_i)$, is in the 4.4−5.1 range for the three compounds (Table 1). Thus, at pH values below ∼3, the acid form is effectively the only species present in the ground state for both nonequilibrated and equilibrated solutions.

The fluorescence spectra of 3-OHF, 4′-HHF, and 6-HHMF in 0.10 M SDS, measured as a function of the aqueous-phase pH with excitation at λ_{exc} = 428, 449, and 431 nm, respectively, exhibit the emission of AH^{+*} and A* (Figure 2), with maxima at the wavelengths listed in Table 1. The corresponding excitation spectra, collected at the emission maxima of AH^{+*} and A* (in solutions with pH ≪ pK_a), are essentially identical to the absorption spectrum of the AH^+ form. This confirms that A* is formed via deprotonation of AH^+ in the excited state, as observed with other flavylium salts in water[28,31] and in micellar media.[30,32]

Time-Resolved Fluorescence. Figure 3 shows tri- and tetraexponential global fits of the fluorescence decays of 3-OHF at 506 nm (emission of AH^{+*}) and 610 nm (emission of A*) in 0.10 M SDS, pH 1.2, at 293 K, with excitation at 424 nm. Clearly, a sum of three exponential terms is insufficient to fit the decay data.[33] Identical observations were made for all decays measured within the pH (1.0−4.6) and temperature (293−318 K) ranges investigated. Figure 4 shows plots of the decay times and preexponential coefficients measured at the emission wavelengths of AH^{+*} and A* as a function of the aqueous phase [H^+]. Table 2 collects this data at three pH values.

The four decay times do not change appreciably between pH 1.0 and 4.45 (Figure 4a). The two shortest decay times (τ_4 and τ_3) appear as rise times (negative preexponential coefficients) at the emission wavelength of A*, consistent with the formation of this species from AH^{+*} in the excited state (Figure 4c). The values of τ_2 are slightly shorter than the lifetimes of the base form of the three compounds (Table 2), measured from single exponential decays at pH ∼ 10. The sum of preexponential coefficients at this wavelength, $\sum A_{2i}$, is equal to zero after correction for the contribution from residual emission of AH^{+*} at 610 nm. This shows that A* is formed totally at the expense of AH^{+*}.

Tetraexponential decays were also required to fit the fluorescence decays of 4′-HHF at 506 nm (emission of AH^{+*}) and 612 nm (emission of A*) in 0.10 M SDS at 293 K, with excitation at 423 nm, at all pH values (Figure 5 and selected data in Table 2). These results led us to redetermine the fluorescence decays of 6-HHMF, which had been measured with inferior time resolution employing our former SPC setup (fwhm

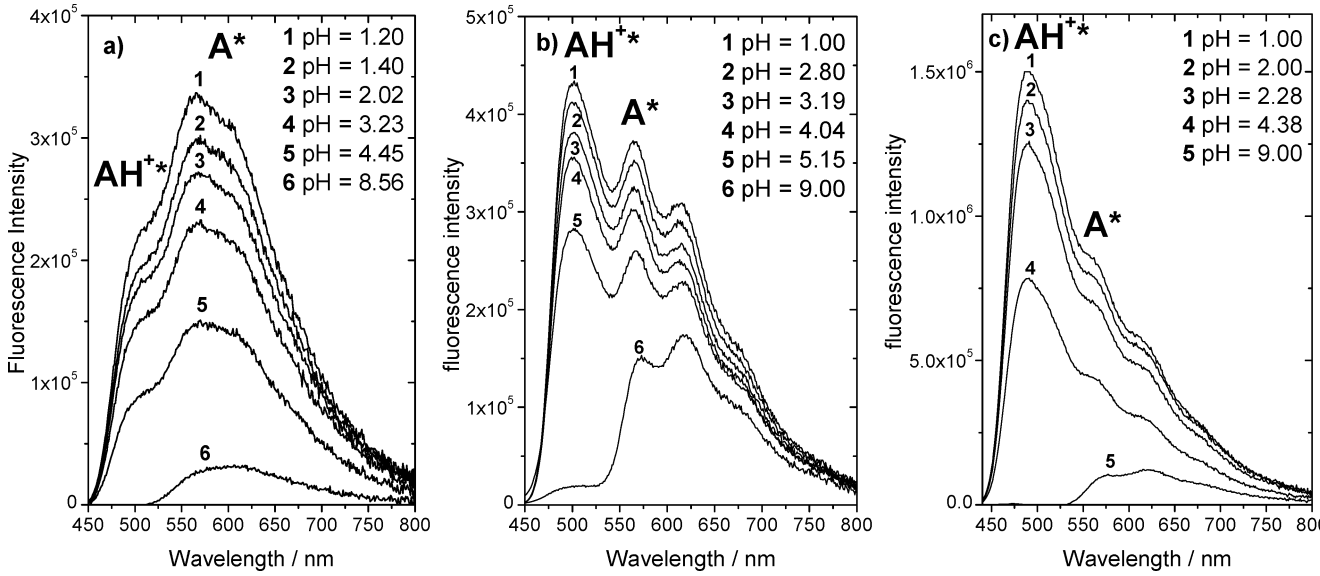

Figure 2. Fluorescence spectra of equilibrated solutions of (a) 3-OHF (λ_{exc} = 428 nm), (b) 4′-HHF (λ_{exc} = 449 nm), (c) 6-HHMF[8] (λ_{exc} = 431 nm) in 0.10 M SDS at 20 °C.

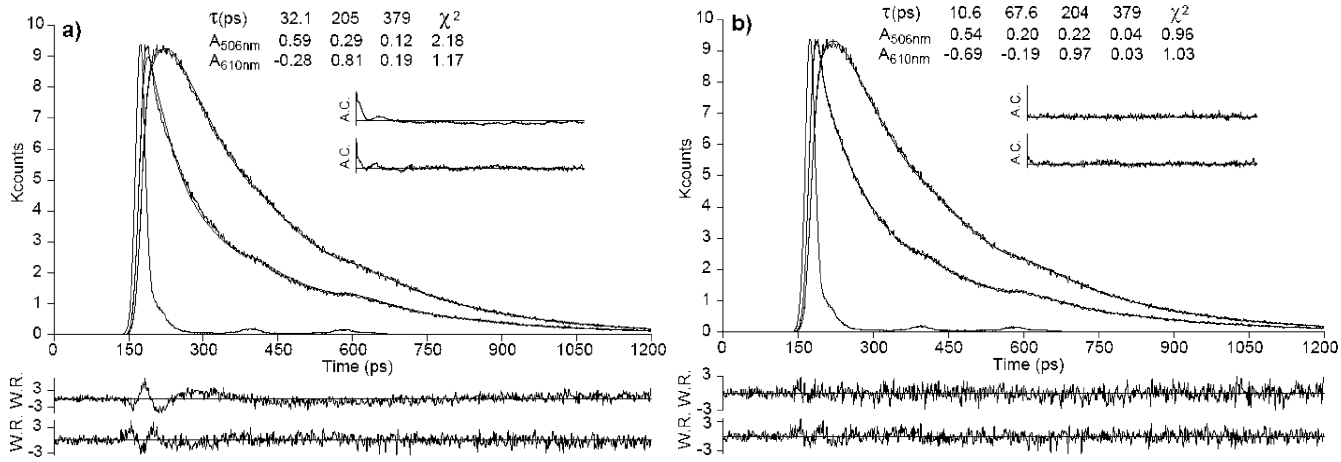

Figure 3. Fluorescence decays of 3-OHF in 0.10 M SDS at pH 1.2 and 293 K measured at 506 nm (acid emission) and 610 nm (base emission) after excitation at 424 nm (pulse). Also shown are the (a) tri- and (b) tetraexponential global fits and the resulting values for decay times (τ_i), normalized preexponential coefficients (A_i) and chi-squared (χ^2) values, as well as the weighted residuals (WR) and autocorrelation functions (AC).

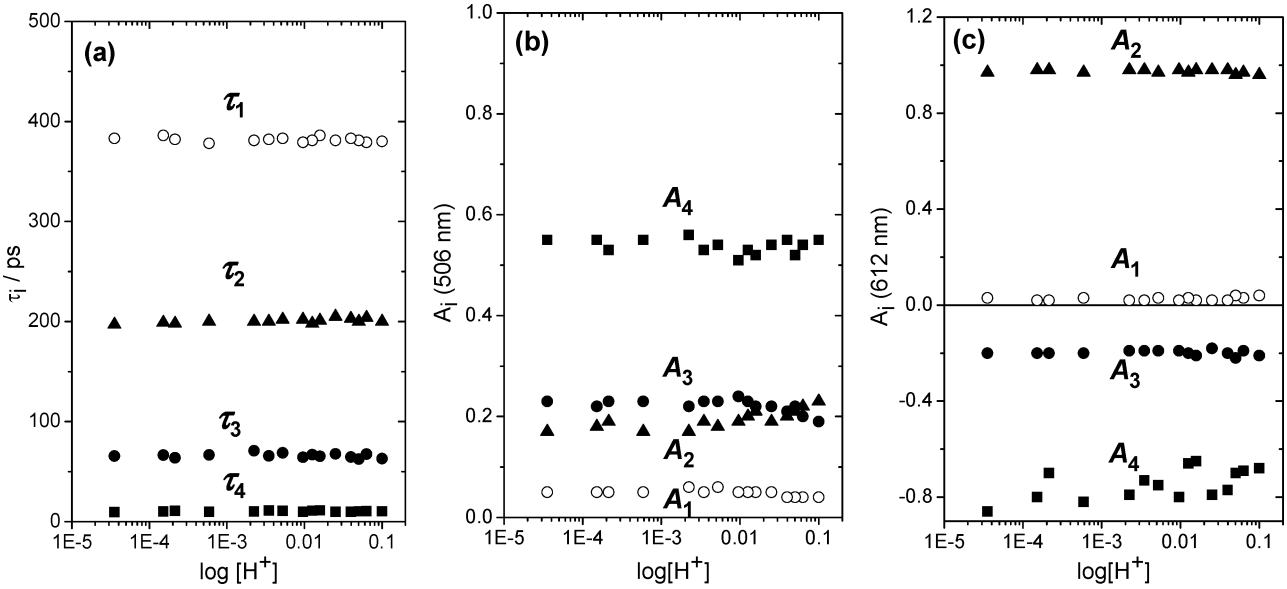

Figure 4. Decay times (a) and pre-exponential coefficients at 506 nm (b) and 610 nm (c) for 3-OHF in 0.10 M SDS as a function of $[H^+]$ in the intermicellar aqueous phase: (□) τ_4 and A_4; (●) τ_3 and A_3; (▲) τ_2 and A_2; (○) τ_1 and A_1.

= 38 ps). Although those previous decays could be acceptably described as the sum of three exponentials,[30] with the better time resolution of our current SPC setup (fwhm = 19 ps), tetraexponential fits of the new decays proved to be better than triexponential fits, the shortest component in the previous triexponential fits now being split into two components (Figure 6 and Table 2).

Temperature Effect on the Fluorescence Decays. The effect of temperature on the decay times of 3-OHF, 4′-HHF, and 6-HHMF in 0.10 M SDS at pH ~3 is shown in Figure 7. The longest decay time, τ_1, is strongly temperature-dependent; τ_2 is less temperature-dependent; and the other two decay times, τ_3 and τ_4, are relatively insensitive to temperature.

Discussion

Data Analysis and Determination of Rate Constants. The fluorescence decays of nonfunctionalized flavylium salts in water are adequately described by the sum of two exponentials, consistent with simple acid−base kinetics (two species, two decay times).[28,29] In SDS micellar solutions, however, the

TABLE 2: Decay Times, τ_i, and Preexponential Coefficients, A_i, at 506 and 610 nm for 3-OHF, 506 and 612 nm for 4′-HHF, and 490 and 620 nm for 6-HHMF in 0.1 M SDS at 293 K at Three Aqueous-Phase pH Values

compound	pH	τ_1/ps	τ_2/ps	τ_3/ps	τ_4/ps	λ_{em}	A_1	A_2	A_3	A_4
3-OHF	1.00	380	200	63	10.4	506	0.04	0.23	0.19	0.55
						610	0.04	0.96	−0.21	−0.68
	2.46	382	200	66	11.2	506	0.05	0.19	0.23	0.53
						610	0.02	0.98	−0.19	−0.73
	4.45	383	197	66	9.5	506	0.05	0.17	0.23	0.55
						610	0.03	0.97	−0.20	−0.86
	9.80		199			610	0	1.00	0	0
4′-HHF	1.00	770	377	79	10.5	506	0.15	0.17	0.17	0.51
						612	0.05	0.95	−0.16	−0.62
	2.37	829	357	73	10.2	506	0.15	0.14	0.18	0.53
						612	0.04	0.96	−0.15	−0.54
	4.04	815	352	73	10.2	506	0.14	0.13	0.18	0.55
						612	0.04	0.96	−0.14	−0.56
	10.81		314			612	0	1.00	0	0
6-HHMF	1.00	1075	277	48	8.6	490	0.28	0.12	0.18	0.41
						620	0.03	0.97	−0.23	−0.53
	2.62	1082	259	57	8.9	490	0.27	0.10	0.17	0.46
						620	0.03	0.97	−0.23	−0.57
	4.38	1086	258	53	8.7	490	0.26	0.11	0.17	0.47
						620	0.03	0.97	−0.23	−0.50
	10.64		258			620	0	1.00	0	0

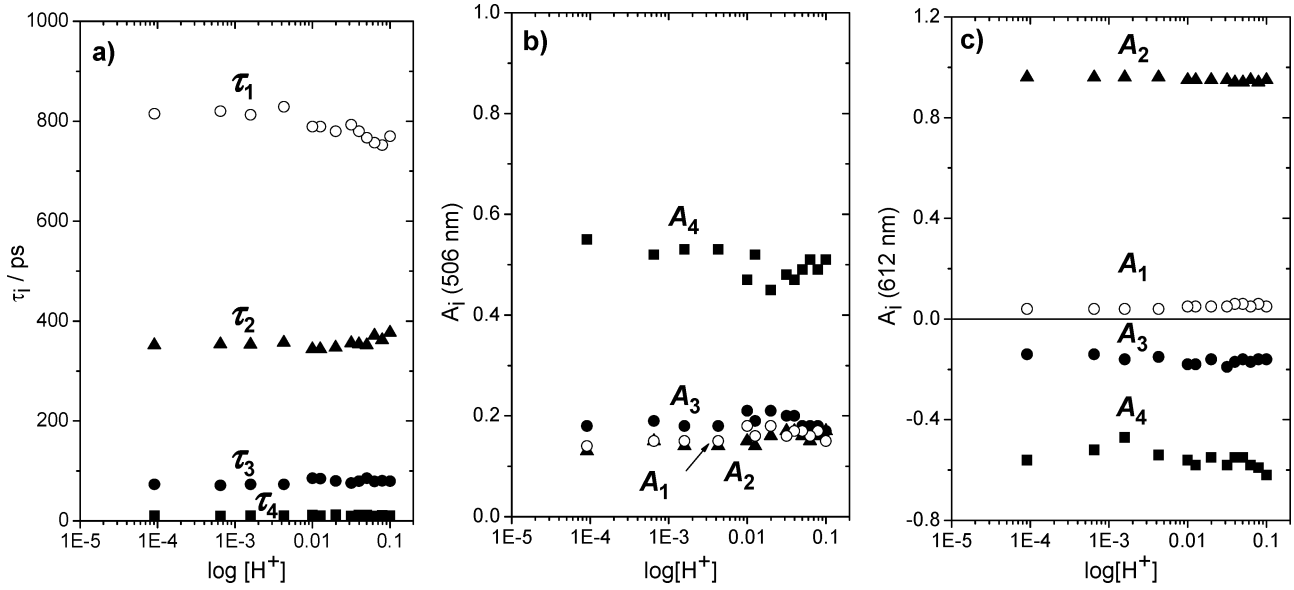

Figure 5. Decay times (a) and preexponential coefficients at 506 nm (b) and 612 nm (c) for 4′-HHF in 0.10 M SDS as a function of $[H^+]$ in the intermicellar aqueous phase: (□) τ_4 and A_4, (●) τ_3 and A_3, (▲) τ_2 and A_2, (○) τ_1 and A_1.

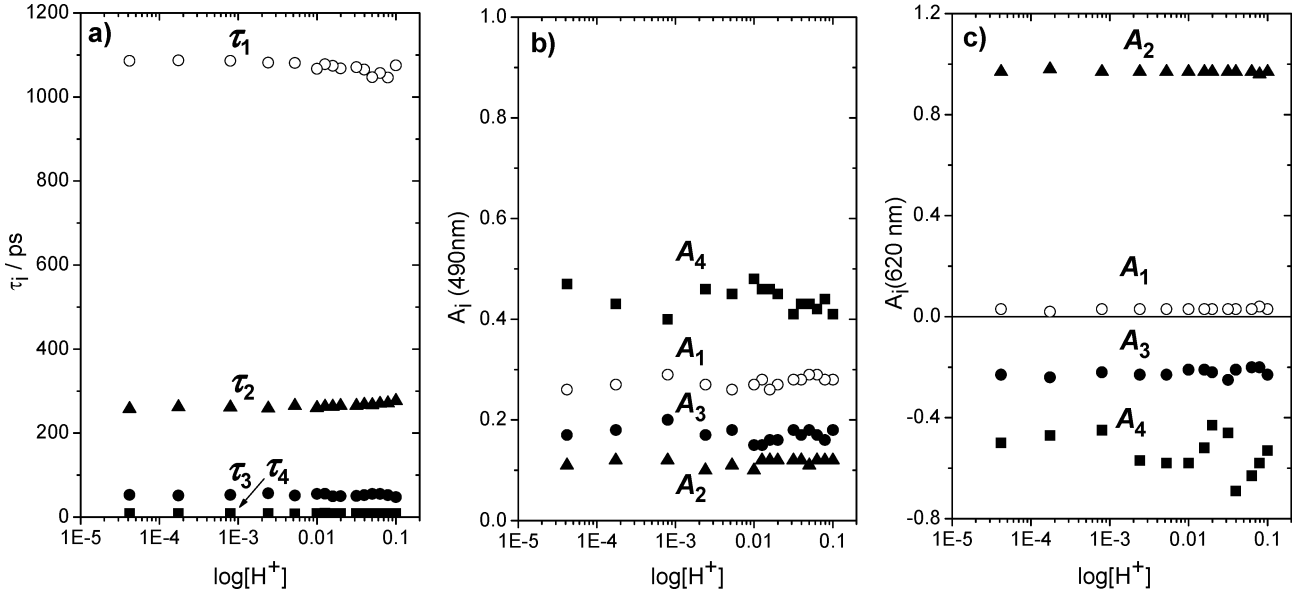

Figure 6. Decay times (a) and preexponential coefficients at 490 (b) and 620 nm (c) for 6-HHMF in 0.10 M SDS as a function of $[H^+]$ in the intermicellar aqueous phase: (□) τ_4 and A_4, (●) τ_3 and A_3, (▲) τ_2 and A_2, (○) τ_1 and A_1.

fluorescence decays of flavylium salts[30,32] required a third, long-lived exponential term. This third (longest) decay time was assigned to emission from a fraction of nonpromptly deprotonable orientations of AH^{+}* in the micelle (denominated "hindered", AH_h^{+}*), whereas the intermediate and shortest decay times were assigned to the "normal" double-exponential acid−base kinetics of the promptly deprotonable orientations of AH^{+}* and A* at the micelle surface.[27,28] However, these previous results also showed indirect evidence for the presence of a fourth species, namely, the geminate excited base-proton pair ($A^*\cdots H^+$) formed upon deprotonation of AH^{+}* (Scheme 2). Specifically, the rate of back-protonation of A* remained high and constant, even for very low proton concentrations in water, suggesting that back-protonation arose predominantly from the geminate pair.[30,32]

Because this scheme contains four kinetically coupled species, one would expect to observe tetraexponential fluorescence decays if all four lifetimes were sufficiently distinct. With the previous time resolution of our instrumentation, we indeed failed to resolve the two shortest lifetimes of 6-HHMF in micellar SDS.[30] With the much better time resolution of our current instrumentation, the shortest lifetime splits into two components, clearly indicating the presence of four exponential terms instead of just three, nicely corroborating our previous mechanistic proposal (Scheme 2).

In Scheme 2, α represents the mole fraction of the hindered orientation, AH_h^{+}*; k_{AH^+} and k_A represent the rate constants for fluorescence decay of AH^{+}* and A*; k_{rot} is the rate constant for rotation of the hindered orientation in the micelle; k_{-rot} is the rate constant for the reverse process; k_d is the rate constant for deprotonation of the nonhindered population of AH^{+}*; k_{rec} is the rate constant for geminate back-protonation of A*; k_{diss} is the rate constant for dissociation of the geminate base-proton pair; and k_p represents the rate constant for formation of ($A^*\cdots H^+$) from A* and a compartmentalized proton, k_{pm}, or a

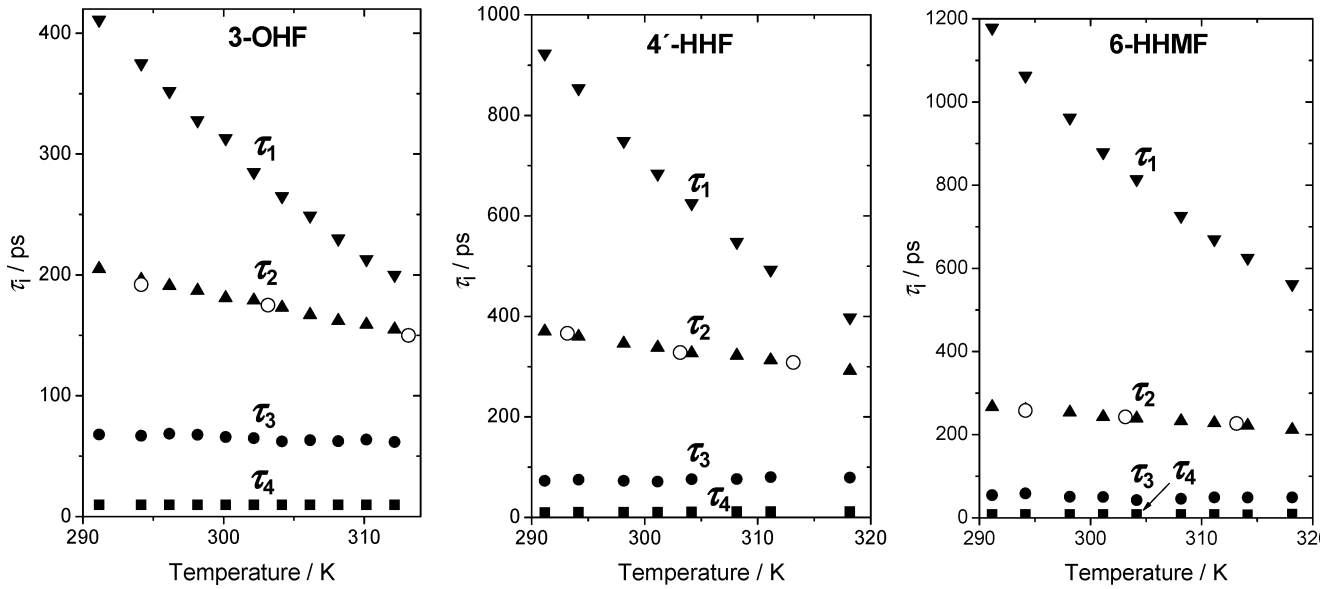

Figure 7. Decay times of 3-OHF (pH = 3.22), 4′-HHF (pH = 3.19), and 6-HHMF (pH = 3.10) in 0.10 M SDS as a function of temperature. Open circles (○) are the lifetimes of the base form measured at pH 10.

SCHEME 2

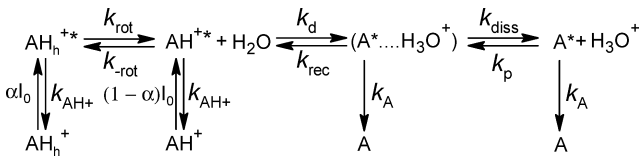

proton arriving from the intermicellar aqueous phase, $k_{pw}[H^+]_w$ (where $k_p = k_{pm} + k_{pw}[H^+]_w$).

As shown in the Supporting Information, the mechanism of Scheme 3 leads to eq 1, the eigenvalues of which correspond to the reciprocals of the four decay times, $\lambda_i = 1/\tau_i$,

$$\begin{vmatrix} \lambda - W & k_{-rot} & 0 & 0 \\ k_{rot} & \lambda - X & k_{rec} & 0 \\ 0 & k_d & \lambda - Y & k_p \\ 0 & 0 & k_{diss} & \lambda - Z \end{vmatrix} = 0 \qquad (1)$$

where W, X, Y, and Z are, respectively, the sums of the rate constants for the decay processes of AH_h^{+}*, AH^{+}*, (A*•••H^+), and A*.

$$W = k_{AH^+} + k_{rot} \qquad (2)$$

$$X = k_{AH^+} + k_d + k_{-rot} \qquad (3)$$

$$Y = k_A + k_{rec} + k_{diss} \qquad (4)$$

$$Z = k_A + k_p \qquad (5)$$

The kinetic analysis, which also requires the use of the values of the preexponential coefficients, can be substantially improved by independently measuring the lifetime of the base (= $1/k_A$) in solutions of sufficiently high pH and the lifetime of the acid in the absence of the proton transfer process (= $1/k_{AH^+}$), taken to be equal to the lifetime of the analogous but nondeprotonable 7-methoxy-4-methyl-flavylium ion.[22,23] The average values of the rate constants at 20 °C derived from this analysis are collected in Table 3. Similar analysis of the data at different temperatures permits evaluation of the temperature dependences of the rate constants, shown as Arrhenius plots in Figure 8, and of the corresponding activation energies presented in Table 3.

Micelle-Anchoring and Orientation of the Probes. One of the particularly interesting features of the flavylium salts is the fact that, in micellar SDS, one can actually detect two distinct populations of the excited acid form at the moment of excitation (Scheme 3). The data for the three micelle-anchored photoacids studied here thus provide unique insight into the extent to which attachment of an alkyl chain to a chromophore does, in fact, allow one to manipulate its preferential orientation in a micelle. Qualitatively, at least, one would anticipate that attachment of a chain at the 3-position would tend to direct the 7-hydroxy group outward much better than attachment of the chain to the 4′-position, which in turn should be preferable to attachment at the 6-position. Indeed, the mole fractions of hindered conformation of the acid at the moment of excitation do increase from 0.05 for 3-OHF to 0.11 for 4′-HHF to 0.24 for 6-HHMF. The rate constants for conversion from the hindered to the nonhindered conformation (k_{rot}) decrease, and those for the reverse process (k_{-rot}) increase in the same order for these three compounds. The general effect of anchoring is indicated by the fact that, in all cases, the fraction of the hindered orientations is substantially less in the anchored anthocyanins than was found for the nonanchored analog HMF (~0.45). In all cases, the activation energies for rotational reorientation of the chromophore, E_{rot} and E_{-rot} (Table 3), are large and consistent with the range of effective local viscosities (14−19 cP) estimated for SDS micelles.[35]

Picosecond Kinetics of the Micelle-Anchored Photoacids. As noted above, excitation of the nonhindered orientations of the acid form of the flavylium salts leads to ultrafast deprotonation in about 10 ps (corresponding to τ_4, Table 2), forming the conjugate base A* at the micelle surface, whose lifetime is on the order of 200−350 ps (corresponding to τ_2, Table 2). Clearly, however, there are two species that are spectroscopically identifiable as A* but kinetically distinct, one of which is formed directly by the ultrafast

SCHEME 3: Representation of the Two Distinct Populations of the Excited Acid Form of the 3-OHF (at the moment of excitation) and the Following Transformations

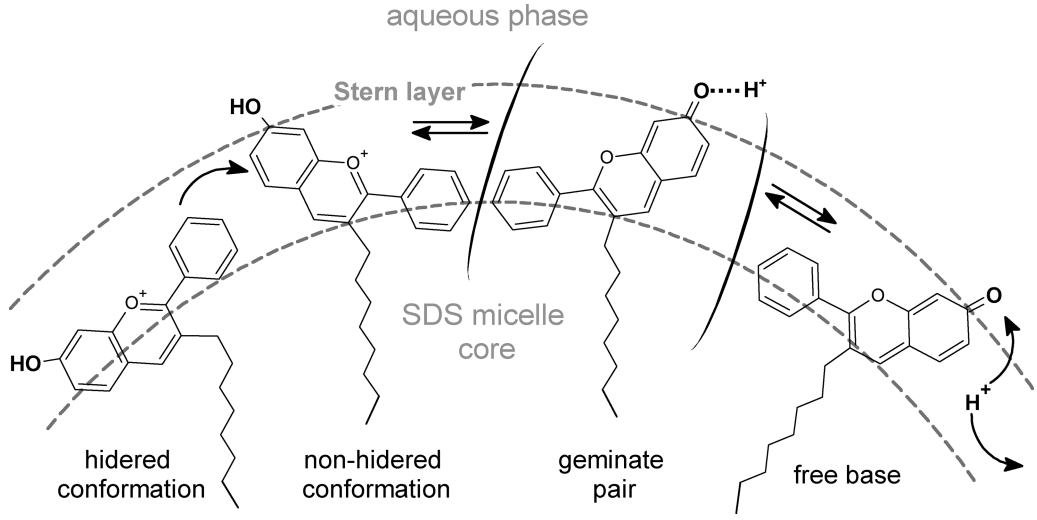

TABLE 3: Rate Constants at 20°C (in ns^{-1}) and Activation Energies (in kJ/mol) of the Kinetic Processes in the First Excited Singlet State of Flavylium Salts in 0.10 M SDS

	3-OHF		4′-HHF		6-HHMF	
rate constant/process	K, ns^{-1}	E_a, kJ/mol	K, ns^{-1}	E_a, kJ/mol	K, ns^{-1}	E_a, kJ/mol
rotation of uncoupled (AH_h^+)* (k_{rot})	1.6	27 ± 2	1.1	26 ± 2	0.8	23 ± 2
back-rotation of (AH^+)* (k_{-rot})	0.08	27 ± 2	0.13	27 ± 2	0.24	25 ± 2
deprotonation of (AH^+)* (k_d)	64	0 ± 1	64	0 ± 1	73	1.7 ± 1
geminate recombination of (A*···H^+) (k_{rec})	28	0 ± 1	29	0 ± 1	35	0.5 ± 1
dissociation of (A*···H^+) (k_{diss})	10	0 ± 1	8.0	0 ± 1	14	0 ± 1
fluorescence decay of A* (k_A)	5.1	10	3.2	6.5	3.9	5.2
rotational equilibrium constant (k_{rot}/k_{-rot})	19		8.1		3.2	
intrinsic efficiency of pair recombination [$k_{rec}/(k_{diss} + k_{rec})$]	0.74		0.78		0.71	
fraction of hindered conformers (α)	0.05		0.11		0.24	
pK_a* from log(k_d/k_{rec})	−0.36		−0.32		−0.32	
compartmentalized protonation (k_{pm})	4.6	0 ± 1	4.4	0 ± 1	7.1	0 ± 1
θ_H-dependent protonation ($k_{p\theta}$)	2.3	0 ± 1	2.6	0 ± 1	2.9	0 ± 1

deprotonation (∼10 ps) and transforms somewhat more slowly into the other (∼70−100 ps, corresponding to τ_3, Table 2). These results are consistent with initial formation of a geminate proton−base pair that subsequently undergoes either geminate recombination to regenerate the acid or transforms into a free base at the micelle surface as the proton migrates away.

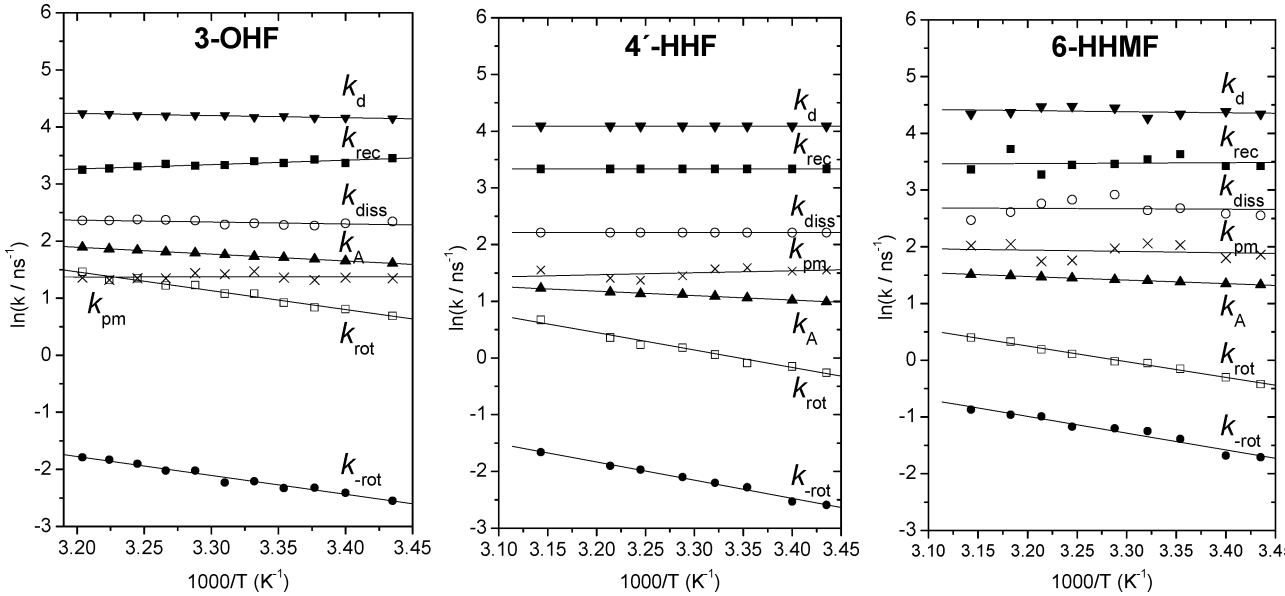

Figure 8. Arrhenius plots of the rate constants (in ns^{-1}) for 3-OHF (pH = 3.22), 4′-HHF (pH = 3.19), and 6-HHMF (pH = 3.10) in 0.10 M SDS solutions: (□) ln(k_{rot}), (●) ln(k_{-rot}), (▲) ln(k_A), (▼) ln(k_d), (□) ln(k_{rec}), (×) ln(k_{pm}), and (○) ln(k_{diss}).

For all three of the photoacids studied here, the initial prompt deprotonation to form the geminate pair occurs at essentially the same rate ($k_d \sim 6-7 \times 10^{10}$ s^{-1}, Table 3). Recombination of the geminate pair is ~3-fold faster than the rate of proton escape from the pair ($k_{rec} \sim 3 \times 10^{10}$ s^{-1} and $k_{diss} \sim 1 \times 10^{10}$ s^{-1}; Table 3), corresponding to an intrinsic recombination efficiency of the pair of ~75%. This high efficiency is consistent with the fact that the protonation reaction of conjugated bases of all flavylium salts studied so far[28,30−32] (and many other conjugated bases of strong photoacids[36]) occurs at essentially the diffusion-controlled rate (values of k_p are typically larger than 2×10^{10} M^{-1} s^{-1} in water at 20 °C for uncharged bases). The ratio of the values of k_d and k_{rec} corresponds to the equilibrium constant for the deprotonation of AH^{+}* to form the geminate pair ($A^{*}\cdots H^{+}$), that is, $K_a^{*} = k_d/k_{rec}$, which is independent of translational diffusion processes and, thus, contains clean information on the energetics of the prototropic process. The values of pK_a* (Table 3) are essentially the same for all three flavylium salts investigated here and correspond to a value of the standard Gibbs energy for proton transfer of $\Delta G^{0}_{pt}{}^{*} = -1.9 \pm 0.1$ kJ/mol. In this context, it should be emphasized that, unlike most other phenolic photoacids, which are either neutral or anionic, the hydroxyflavylium salts are cationic, and the corresponding base is neutral, meaning that electrostatic effects do not contribute directly to the rates of proton dissociation and recombination.

Several studies of the temperature dependence of the excited-state proton transfer reactions of very strong photoacids have shown that the apparent activation barrier decreases with increasing temperature, becoming almost barrierless at and above ambient temperature.[37] This has been attributed to a change from adiabatic to nonadiabatic proton transfer as the temperature is increased.[37] The present results indicate that none of the individual proton transfer steps (k_d, k_{rec}, k_{diss}) of these micelle-anchored flavylium ions has a significant activation barrier.

Diffusional Reprotonation of A* at the Micelle Surface. At first glance (Figures 4b, 5b, and 6b), the value of A_2 in the AH^{+}* decay, which reflects the amount of AH^{+}* resulting from reprotonation of A*, is surprisingly insensitive to the concentration of protons in the intermicellar aqueous phase, even at an intermicellar pH of 1. Since diffusion-mediated protonation at the surface of an anionic micelle is presumably a two-step process in which the proton is captured by the electrostatic field of the micelle and then migrates in the Stern layer until it finds the base,[38,39] we plot in Figure 9 the net rate constant for protonation, k_p, as a function of the fractional degree of coverage of the micelle surface by protons, θ_H. Because the selectivity coefficient for proton/sodium counterion exchange at the SDS micellar surface is unity,[38] θ_H can be readily calculated from the relationship $\theta_H = [H^{+}]_{tot}/([H^{+}]_{tot} + [Na^{+}]_{tot})$, where $[H^{+}]_{tot}$ and $[Na^{+}]_{tot}$ are, respectively, the total concentrations of protons and of sodium ions present in the solution. As shown in Figure 9, these plots are reasonably linear, corresponding to the function $k_p = k_{pm} + k_{p\theta} \times \theta_H$.

By analogy to rate constants for quenching of the fluorescence of aromatic molecules by quencher counterions,[39] the value of $k_{p\theta}$ has a readily interpretable significance and corresponds to the net rate constant for diffusion-mediated protonation of the base at unit coverage of the micelle surface by protons. The corresponding intramicellar rate constant, k_{qH}, for diffusion-mediated protonation in a micelle containing a single, randomly distributed proton can then be estimated by dividing $k_{p\theta}$ by the SDS micellar aggregation number (~90−95 monomers/micelle at our ionic strength[40]). The values of $k_{p\theta}$, $\sim 2.5 \times 10^{9}$ s^{-1} for the three probes, correspond to a value of k_{qH} of $\sim 3 \times 10^{7}$ s^{-1}, which is a typical value for diffusion-controlled quenching of fluorescence probes by quenchers in SDS micelles.[39] The lack of a more pronounced dependence of k_p on the intermicellar proton concentration is thus merely a reflection of the very short, subnanosecond lifetime of the excited base and not of any kinetic anomaly in the rates of proton migration between the aqueous phase and the micelle.

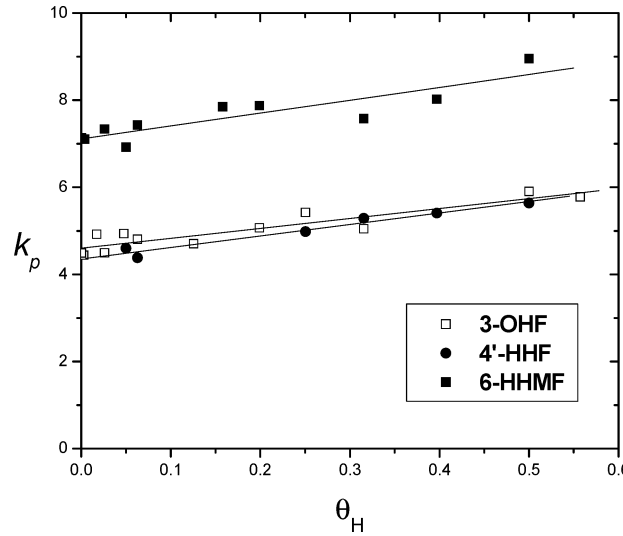

Figure 9. Plot of the net protonation rate constant, k_p values as a function of θ_H, the fractional coverage of the SDS micellar surface by protons at 293 K.

Geminate Reprotonation at the Micelle Surface. Although this provides a reasonable explanation for the rather small dependence of k_p on the external proton concentration, it does not address the question of the origin of the dominant pH-insensitive contribution to the rate constant, that is, k_{pm}. The most logical explanation in this case is that proposed by Huppert and co-workers,[3,4] that is, that partial separation of the initially formed contact pair ($A^{*}\cdot\cdot H^{+}$) leads to the solvent-separated pair $\{A^{*}-H^{+}\}_{mic}$ that is still in effect partially compartmentalized at the micelle surface. Thus, on the very fast time scale dictated by the lifetime of the excited base, reprotonation by the proton produced by the initial photoinduced deprotonation continues to be the dominant contributor to the reprotonation process in the solvent-separated pair, although at a slower rate than geminate recombination in the initially formed pair (by a factor of 5−10 in the present case).

Nonetheless, this does not adequately address the question of why we observe compartmentalization at the micellar surface, but not in bulk solution, where simple two-species (acid + base) kinetics prevail. The rationalization of this difference derives from the recognition that the initial proton transfer occurs not to a monomeric water molecule, but rather, to an extended water network. In bulk water, proton transfer through the network leads to efficient escape of the proton out into the solution, particularly when the water network is interrupted via hydrogen bond fluctuations. However, in the presence of high concentrations of anions, long-range proton transfer via hydrogen-bonded water bridges that connect the photoacid to a nearby anion can, in some cases, be an important secondary contributor to the proton transfer process.[14,15,41] At the micelle surface, water is more structured than in the bulk, and the local concentration of surfactant anionic headgroups is quite substantial (2−3 M) in the Stern layer surrounding the cationic photoacid.[20,38] In effect,

then, the observation of ultrafast transfer of the proton to water and of substantial compartmentalization of the photogenerated proton at the micelle surface on the picosecond time scale strongly suggests preferential transfer of the proton to preformed hydrogen-bonded water bridges between the photoacid and the anionic headgroups. These protonated water bridges localize the proton in the vicinity of the excited base much more efficiently than in bulk water, resulting in the predominance of geminate reprotonation at the micelle surface.

Acknowledgment. This work was supported by Fundação para a Ciência e Tecnologia (FCT), Portugal (Project PTDC/QUI/65728/2006) and a CAPES-GRICES International Cooperation Grant. F.H.Q. thanks the Conselho Nacional de Desenvolvimento Científico e Tecnológico (CNPq) for funding (Projeto Universal) and fellowship support. A.A.F. thanks the FCT for the postdoctoral grant SFRH/BPD/34820/2007. The authors thank Drs. Klaas Zachariasse and Sergey Druhizin (Max-Planck-Institut für Biophysikalische Chemie, Göttingen, Germany) for kindly confirming the presence of the two shortest lifetime components in the decays of 3-OHF.

Supporting Information Available: The detailed kinetic treatment of the collected data. This information is available free of charge via the Internet at http://pubs.acs.org.

References and Notes

(1) Shizuka, S.; Tobita, S. In *Organic Photochemistry and Photophysics. Molecular and Supramolecular Photochemistry*; Ramamurthy, V.; Schanze, K. S., Eds.; CRC Press/Taylor & Francis: Boca Raton, FL, 2006; Vol. 14, pp 37−74.

(2) Agmon, N. *J. Phys. Chem. A* **2005**, *109*, 13–35.

(3) Leiderman, P.; Genosar, L.; Huppert, D. *J. Phys. Chem. A* **2005**, *109*, 5965–5977.

(4) Gepshtein, R.; Leiderman, P.; Genosar, L.; Huppert, D. *J. Phys. Chem. A* **2005**, *109*, 9674–9684.

(5) Pérez-Lustres, J. L.; Rodriguez-Prieto, F.; Mosquera, M.; Senyushkina, T. A.; Ernsting, N. P.; Kovalenko, S. A. *J. Am. Chem. Soc.* **2007**, *129*, 5408–5418.

(6) Silverman, L. N.; Spry, D. B.; Boxer, S. G.; Fayer, M. D. *J. Phys. Chem. A* **2008**, *112*, 10224–10249.

(7) Spry, D. B.; Fayer, M. D. *J. Chem. Phys.* **2008**, *128*, 084508.

(8) Kaneko, S.; Yotoriyama, S.; Koda, H.; Tobita, S. *J. Phys. Chem. A* **2009**, *113*, 3021–3028.

(9) Ghosh, S.; Dey, S.; Mandal, U.; Adhikari, A.; Mondal, S. K.; Bhattacharyya, K. *J. Phys. Chem. B* **2007**, *111*, 13504–13510.

(10) Ghosh, S.; Mandal, U.; Adhikari, A.; Dey, S.; Bhattacharyya, K. *Int. Rev. Phys. Chem.* **2007**, *26*, 421–448.

(11) Sahu, K.; Roy, D.; Mondal, S. K.; Karmakar, R.; Bhattacharyya, K. *Chem. Phys. Lett.* **2005**, *404*, 341–345.

(12) See, however, ref 7 and (a) Mohammed, O. F.; Dreyer, J.; Magnes, B.-Z.; Pines, E.; Nibering, E. T. J. *Chem. Phys. Chem.* **2005**, *6*, 625. (b) Spry, D. B.; Goun, A.; Glusac, K.; Moilanen, D. E.; Fayer, M. D. *J. Am. Chem. Soc.* **2007**, *129*, 8122. (c) Silverman, L. N.; Spry, D. B.; Boxer, S. G.; Fayer, M. D. *J. Phys. Chem. A* **2008**, *112*, 10244–10249. (cc) Tielrooij, K. J.; Cox, M. J.; Bakker, H. J. *Chem. Phys. Chem.* **2009**, *10*, 245.

(13) Georgieva, I.; Trendafilova, N.; Aquino, A. J. A.; Lischka, H. *J. Phys. Chem. A* **2007**, *111*, 127–135.

(14) Mancinelli, R.; Sodo, A.; Bruni, F.; Ricci, M. A.; Soper, A. *J. Phys. Chem. B* **2009**, *113*, 4075–4081.

(15) Cox, J. C.; Siwick, B. J.; Bakker, H. J. *Chem. Phys. Chem.* **2009**, *10*, 236–244.

(16) Marx, D. *Chem. Phys. Chem.* **2006**, *7*, 1848–1870.

(17) Chandra, A.; Tuckerman, M. E.; Marx, D. *Phys. Rev. Lett.* **2007**, *99*, 145901.

(18) Markovich, O.; Chen, H.; Izvekov, S.; Paesani, F.; Voth, G. A.; Agmon, N. *J. Phys. Chem. B* **2008**, *112*, 9456–9466.

(19) Iuchi, S.; Chen, H.; Paesani, F.; Voth, G. A. *J. Phys. Chem. B* **2009**, *113*, 4017–4030.

(20) El Seoud, O. A. *J. Mol. Liq.* **1997**, *72*, 85–103.

(21) Fernandes, A. C.; Romão, C. C.; Rosa, C. P.; Vieira, V. P.; Lopes, A.; Silva, P. F.; Maçanita, A. L. *Eur. J. Org. Chem.* **2004**, *23*, 4877–4883.

(22) Silva, P. F.; Lima, J. C.; Quina, F. H.; Maçanita, A. L. *J. Phys. Chem. A* **2004**, *107*, 3263–3269.

(23) Rodrigues, R.; Silva, P. F.; Shimizu, K.; Freitas, A. A.; Kovalenko, S. A.; Ernsting, N. P.; Quina, F. H.; Maçanita, A. L. *Chem.—Eur. J.* **2009**, *15*, 1397–1402.

(24) Striker, G.; Subramaniam, V.; Seidel, C. A. M.; Volkmer, A. J. *J. Phys. Chem. B* **1999**, *103*, 8612–8617.

(25) (a) Brouillard, R. In *Anthocyanins as Food Colors*; Markakis, P., Ed.; Academic Press: New York, 1982; Chapter 1. (b) Brouillard, R. *Phytochemistry* **1981**, *20*, 143–145. (c) Brouillard, R.; Dubois, J.-E. *J. Am. Chem. Soc.* **1977**, *99*, 1359–1364. (d) Brouillard, R.; Delaporte, B.; Dubois, J.-E. *J. Am. Chem. Soc.* **1978**, *100*, 6202–6205.

(26) Santos, H.; Turner, D. L.; Lima, J. C.; Figueiredo, P.; Pina, F.; Maçanita, A. L. *Phytochemistry* **1993**, *33*, 1227–1232.

(27) Maçanita, A. L.; Moreira, P. F.; Lima, J. C.; Quina, F. H.; Yihwa, C.; Vautier-Giongo, C. *J. Phys. Chem. A* **2002**, *106*, 1248–1255.

(28) (a) Paulo, L.; Freitas, A. A.; Silva, P. F.; Shimizu, K.; Quina, F. H.; Maçanita, A. L. *J. Phys. Chem. A* **2006**, *110*, 2089–2096. (b) Moreira, P. F.; Giestas, L.; Yihwa, C.; Vautier-Giongo, C.; Quina, F. H.; Maçanita, A. L.; Lima, J. C. *J. Phys. Chem. A* **2003**, *107*, 4203–4210.

(29) (a) Lima, J. C.; Vautier-Giongo, C.; Lopes, A.; Melo, E. C.; Quina, F. H.; Maçanita, A. L. *J. Phys. Chem. A* **2002**, *106*, 5851–5859. (b) Vautier-Giongo, C.; Yihwa, C.; Moreira, P. F.; Lima, J. C.; Freitas, A. A.; Quina, F. H.; Maçanita, A. L. *Langmuir* **2002**, *18*, 10109–10115.

(30) Rodrigues, R.; Vautier-Giongo, C.; Silva, P. F.; Fernandes, A. C.; Cruz, R.; Maçanita, A. L.; Quina, F. H. *Langmuir* **2006**, *22*, 933–940.

(31) Lima, J. C.; Abreu, I.; Santos, H.; Brouillard, R.; Maçanita, A. L. *Chem. Phys. Lett.* **1998**, *298*, 189–195.

(32) (a) Giestas, L.; Yihwa, C.; Lima, J. C.; Vautier-Giongo, C.; Lopes, A.; Quina, F. H.; Maçanita, A. L. *J. Phys. Chem. A* **2003**, *107*, 3263–3267. (b) Freitas, A. A.; Paulo, L.; Maçanita, A. L.; Quina, F. H. *Langmuir* **2006**, *22*, 7986–7993.

(33) The current systems fall into the A−B limit of Gopich et al.,[34] where the decays become purely exponential. To convince ourselves that the decays were, indeed, tetraexponential, the fluorescence decays of 3-OHF were also measured by picosecond TCSPC in Klaas Zachariasse's laboratory (see the Acknowledgements), with identical results. The capability of the MPI equipment to measure decay times as short as 3 ps has been shown in a substantial number of publications, where these short times were confirmed using femtosecond time-resolved absorption (Niko Ernsting's laboratory at the University of Berlin). With our current TCSPC equipment (now 17−18 ps fwhm), we measure 4.5 ps for the shortest decay time of the nonfunctionalized parent photoacid 4-methyl-7-hydroxyflavylium in water, as compared to 4.2 ps using femtosecond time-resolved absorption at Fausto Elisei's laboratory in Perugia.

(34) Gopich, I. V.; Solntsev, K. M.; Agmon, N. *J. Chem. Phys.* **1999**, *110*, 2164–2174.

(35) (a) Zachariasse, K. A. *Chem. Phys. Lett.* **1978**, *57*, 429–432. (b) Maiçanita, A. L. Ph.D. Thesis; Ed. I.S.T. Universidade Técnica de Lisboa, Portugal, 1981, p 245.

(36) Arnaut, L. G.; Formosinho, S. *J. Photochem. Photobiol., A* **1993**, *75*, 1–20.

(37) (a) Cohen, B.; Leiderman, P.; Huppert, D. *J. Phys. Chem. A* **2002**, *106*, 11115–11122. (b) Cohen, B.; Leiderman, P.; Huppert, D. *J. Phys. Chem. A* **2003**, *107*, 1433–1440.

(38) Bunton, C. A.; Nome, F.; Quina, F. H.; Romsted, L. S. *Acc. Chem. Res.* **1991**, *24*, 357–364.

(39) (a) Quina, F. H.; Lissi, E. A. *Acc. Chem. Res.* **2004**, *37*, 703–710. (b) Gehlen, M. H.; De Schryver, F. C. *Chem. Rev.* **1993**, *93*, 199–221. (c) Alonso, E. O.; Quina, F. H. *Langmuir* **1995**, *11*, 2459–2463.

(40) Quina, F. H.; Nassar, P. M.; Bonilha, J. B. S.; Bales, B. L. *J. Phys. Chem.* **1995**, *99*, 17028–17031.

(41) For simulations of proton transport and diffusion at memebrane surfaces, see: (a) Smondyrev, A. M.; Voth, G. A. *Biophys. J.* **2002**, *82*, 1460–1468. (b) Georgievskii, Y.; Medvedev, E. S.; Stuchebrukhov, A. A. *Biophys. J.* **2002**, *82*, 2833–2846.

JP100281U